Carboxylic Group and Its Tetrazolyl Isostere in One Molecule. Matrix Isolation FTIR and DFT Studies on Thermal Decomposition and Photochemistry of (Tetrazol-5-yl)acetic Acid

ARTICLE *in* THE JOURNAL OF PHYSICAL CHEMISTRY A · MARCH 2014

Impact Factor: 2.69 · DOI: 10.1021/jp5001804 · Source: PubMed

3 AUTHORS:

Magdalena Pagacz-Kostrzewa
University of Wroclaw
9 PUBLICATIONS **60** CITATIONS
SEE PROFILE

Justyna Alicja Krupa
University of Wroclaw
7 PUBLICATIONS **23** CITATIONS
SEE PROFILE

Maria Wierzejewska
University of Wroclaw
61 PUBLICATIONS **475** CITATIONS
SEE PROFILE

THE JOURNAL OF PHYSICAL CHEMISTRY A

Article

pubs.acs.org/JPCA

Carboxylic Group and Its Tetrazolyl Isostere in One Molecule. Matrix Isolation FTIR and DFT Studies on Thermal Decomposition and Photochemistry of (Tetrazol-5-yl)acetic Acid

M. Pagacz-Kostrzewa, J. Krupa, and M. Wierzejewska*

Faculty of Chemistry, University of Wrocław, Joliot-Curie 14, 50-383 Wrocław, Poland

Supporting Information

ABSTRACT: The title compound (tetrazol-5-yl)acetic acid (TA) is an interesting molecule that contains both a carboxylic group and its isostere tetrazolyl group. Out of nine theoretically predicted stable structures of TA, three appeared to be present in solid argon. Thermal decomposition of the species aided by water molecules was studied in detail both experimentally using FTIR matrix isolation technique and theoretically at the B3LYP/6-311++G(2d,2p) level. Experimentally, it was found that the decarboxylation process appeared at the presence of water traces in the system. Theoretically, it was shown that the energy barrier of the water assisted process was lower by ca. 30 kJ mol^{-1} comparing to the process without water participation. The UV photolysis of the TA/Ar system was studied using both broad-band and narrow-band sources. The main photoproducts appeared to be carbodiimidylacetic acid and (1*H*-diaziren-3-yl)acetic acid. The progress of the reactions induced was followed by FTIR spectroscopy, whereas interpretation of the results was supported by quantum chemical calculations (DFT, TD-DFT).

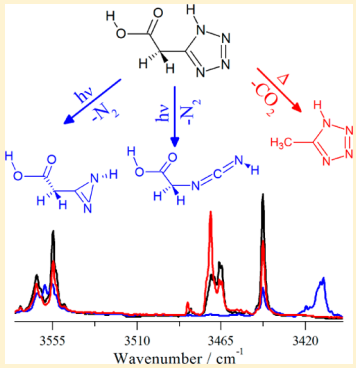

1. INTRODUCTION

Tetrazole derivatives have drawn attention of chemists due to their diverse practical applications as environmentally friendly energetic materials[1−5] and valuable ligands in coordination chemistry forming new topologies and exhibiting interesting properties such as spin-crossover phenomena.[6,7] However, the most spectacular are applications of tetrazoles in medicine and pharmacy.[8−10] Many of the medicinal applications of tetrazole derivatives originate from the properties of the tetrazolic acid fragment CN_4H. It has similar acidity to the carboxylic group, is almost allosteric with it, but is metabolically more stable.[11] Hence, the COOH groups are often replaced by the CN_4H fragments in biologically active molecules and the tetrazole ring is found in drugs or potent medicines with diverse pharmacological activity.[8−10,12−15]

From the fundamental point of view, tetrazole derivatives have been found to be challenging molecules due to their interesting structures (tautomers/conformers) and usually rich photochemistry that strongly depend on the specific substituents attached to the ring. The latter subject has been extensively studied, and both the simplest tetrazole and its different C- or N-substituted derivatives were studied.[16−24] Despite many papers published, the results on the N−H tetrazoles bearing carboxylic group are scarce. Alkorta and Elguero reported DFT calculations carried out on a number of NH-azoles with the COOH substituent.[25] Pagacz-Kostrzewa et al.[26] performed single crystal X-ray diffraction and FTIR studies of the title compound (tetrazol-5-yl)acetic acid (TA) in the crystalline phase. This compound is an interesting example of the 5-substituted tetrazole derivative possessing a free N−H group and the CH_2COOH moiety attached to the tetrazole C atom.

Photochemistry of simple carboxylic acids isolated in low temperature matrices remains of a fundamental interest due to their role in atmospheric and interstellar chemistry as well as their significance in human metabolism.[27−30] Several alternative photolysis channels are usually considered involving either molecular elimination (e.g., CO, CO_2) or generating OH radicals. Molecular complexes between different photoproducts are often formed as well.

The goal of the present work was to identify and characterize different isomers of TA and to study their thermal decomposition and UV-induced photochemistry. We have chosen matrix isolation FTIR spectroscopy as the main experimental technique, since it is especially powerful in conformational studies and in the identification of the photolysis and pyrolysis or thermal decomposition products.[24−35] Interpretation of the spectroscopic results was supported by extensive DFT calculations.

2. EXPERIMENTAL SECTION

2.1. Matrix Isolation Studies. In order to obtain matrices containing TA, the crystalline sample was placed in a small electric oven located inside the vacuum vessel of the cryostat near the cold window. Different experiments were performed during which the sample was allowed to sublimate at the

Received: January 7, 2014
Revised: February 21, 2014
Published: March 11, 2014

dx.doi.org/10.1021/jp5001804 | J. Phys. Chem. A 2014, 118, 2072−2082

temperature interval 330−350 K. The temperature of the oven was controlled by the DC regulated power supply (NDN Instruments) that allowed for the precise regulation of the current. The vapor of TA was deposited onto a cold CsI window with a large excess of matrix gas. The cold window was maintained at a temperature 15/11 K (deposition/measurement) by means of a closed cycle helium refrigerator (ARS-2HW). Infrared spectra were recorded between 4000 and 400 cm^{-1} in a transmission mode with a resolution of 0.5 cm^{-1} by means of a Bruker 66 FTIR spectrometer equipped with a liquid N_2 cooled MCT detector.

2.2. Photolysis Experiments. After the infrared spectra of the initially deposited matrices were recorded the samples were irradiated with the high pressure 450 W Xe lamp (Optel ZXE-450) using either series of long-pass optical filters (Schott WG: 435, 394, 345, 320, 305, 295, and 280 nm) or full output power of the lamp. Matrices were also irradiated with the tunable UV light provided by the frequency doubled signal beam of a pulsed (7 ns) optical parametric oscillator Vibrant 355 (Opotek Inc.) (repetition rate 10 Hz) pumped with a pulsed Nd:YAG laser (Quantel). The line width of the output was 4−7 cm^{-1}, while the average pulse energy was ∼4.0 mJ.

2.3. Computational Details. All calculations were performed with the Gaussian 09-D.01 program package.[36] Structures of the minima and transition states were optimized at the B3LYP/6-311++G(2d,2p) level. For reaction paths, minima were connected to each transition state (TS) by following intrinsic reaction coordinate (IRC)[37,38] generated at the same level. The values of relative abundance for the TA isomers were calculated using equation: $\Delta G = -RT \ln K$, where ΔG is the difference between Gibbs free energy for two given isomeric forms and K is the equilibrium constant for these species. The associated force constant matrixes were calculated at the B3LYP/6-311++G(2d,2p) level for all precursors and photoproducts to evaluate harmonic frequencies and zero-point vibrational (ZPE) corrections as well as the corresponding thermodynamic functions. The calculated harmonic frequencies were scaled down to correct them mainly for the effects of basis set limitations, neglected part of electron correlation, and anharmonicity effects. Two different scaling factors were used to reproduce experimental spectra: 0.95 above 2800 cm^{-1} where stronger anharmonicity was expected, and 0.98 below 2800 cm^{-1}. Anharmonic frequencies and intensities were calculated at the same level of theory as well. There were only slight differences between harmonic (scaled) and anharmonic frequencies however better agreement with the experiment for photoproducts was obtained using harmonic (scaled) values. The vertical excitation energies were calculated using the time dependent density functional theory TD-DFT.[39,40] The potential energy distributions (PED) of the normal modes were computed with the GAR2PED program[41] and the vibrational spectra were simulated using SYNSPEC program.[42]

3. RESULTS AND DISCUSSION

3.1. Structures and Relative Energies of the Minima. The (tetrazol-5-yl)acetic acid molecule has three internal rotational degrees of freedom, which may result in the presence of a number of different conformers. In addition, for each conformer there are also two tautomers possible, which differ in the position of the tetrazole-ring hydrogen atom. Out of 24 initially considered forms (conformers and tautomers) 18 appeared to be stable structures. All species have the C_1 symmetry and consist of nine pairs of mirror image structures of the same energy; only one structure of each pair, altogether nine different species, will be considered further. Four of them (1*H*-TA1, 2*H*-TA1, 2*H*-TA2, and 1*H*-TA2) are characterized by a cis configuration of the carboxylic group, whereas the remaining five possess a trans COOH group. Four of the structures (1*H*-TA1, 1*H*-TA2, 1*H*-TA3 and 1*H*-TA4) have tetrazole ring annular hydrogen in the *1-H* position, whereas the *2-H* position occurs in five forms (2*H*-TA1, 2*H*-TA2, 2*H*-TA3, 2*H*-TA4, and 2*H*-TA5). The geometry of the three most stable TA species in two different projections is shown in Figure 1. The remaining geometries are presented in Figure S1

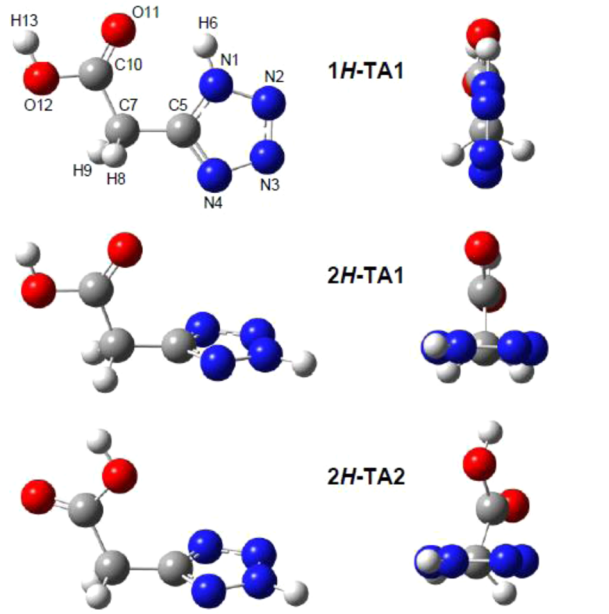

Figure 1. B3LYP/6-311++G(2d,2p) optimized geometry of the three most stable TA species in two different projections.

in the Supporting Information. The key dihedral angles and the dipole moment values of the nine TA species are listed in Table 1. For comparison, the values of the corresponding dihedral angles obtained from the X-ray diffraction[26] are added.

According to the calculations, the most stable form appeared to be almost planar molecule 1*H*-TA1 that is 1*H* tautomer with the carbonyl group in the cis position relative to the N−H

Table 1. Key Dihedral Angles (deg) and Dipole Moment Values (D) of the TA Conformers Calculated at the B3LYP/6-311++G(2d,2p) Level

conformer	$\Phi(N_1C_5C_7C_{10})$	$\Phi(C_5C_7C_{10}O_{11})$	$\Phi(O_{11}C_{10}O_{12}H_{13})$	μ
1*H*-TA1	−5.3	4.4	0.2	6.26
2*H*-TA1	89.3	−4.0	0.0	2.45
2*H*-TA2	107.0	153.6	−0.8	3.34
2*H*-TA3	141.4	−153.0	177.1	6.02
1*H*-TA2	43.9	134.1	−0.7	5.48
1*H*-TA3	157.8	−163.7	177.1	5.36
2*H*-TA5	−38.5	−155.0	177.6	5.15
1*H*-TA4	−11.9	10.3	−178.9	5.41
2*H*-TA4	88.1	−5.2	179.1	4.35
exp[a]	−21.30(8)	7.15(8)		

[a]Reference 26.

dx.doi.org/10.1021/jp5001804 | J. Phys. Chem. A 2014, 118, 2072−2082

bond. This form is stabilized by the intramolecular hydrogen bond with the calculated N···O distance and the N−H···O angle equal to 2.750 Å and 114.6°, respectively.

Next two most stable TA structures (2*H*-TA1, 2*H*-TA2) are characterized by the 2*H* position of the tetrazole ring annular hydrogen and almost perpendicular arrangement of the ring in respect to the COOH plane with the $N_1C_5C_7C_{10}$ dihedral angle values of 89.3° and 107.0°, respectively. 2*H*-TA1 and 2*H*-TA2 are only slightly less stable than 1*H*-TA1 with the calculated relative energy ΔE_{ZPE} equal to 3.86 and 6.54 kJ mol^{-1}, respectively. The remaining six TA minima are clearly less stable with the ΔE_{ZPE} values between 10.33 and 26.74 kJ mol^{-1}. The calculated energetic parameters relative energies and relative Gibbs free energies for nine TA minima are collected in Table 2. Additionally, data obtained for two transition states

Table 2. Relative Energies ΔE, Zero-Point Energy Corrected Relative Energies ΔE_{ZPE}, Relative Gibbs Free Energies ΔG (kJ mol^{-1}) and Abundances A_{342} and A_w (%) for Different TA Isomers and Selected Transition States Calculated at the B3LYP/6-311++G(2d,2p) Level[a]

minima	ΔE	ΔE_{Zpe}	ΔG	A_{342}	A_W
1*H*-TA1	0.00	0.00	0.00	75.7	58.9
2*H*-TA1	2.95	3.86	4.48	15.2	38.5
2*H*-TA2	5.46	6.54	6.49	7.8	2.6
2*H*-TA3	8.03	10.33	13.55	0.5	0.0
1*H*-TA2	12.00	12.13	13.66	0.6	0.0
1*H*-TA3	15.63	16.09	18.33	0.1	0.0
2*H*-TA5	15.04	16.62	18.89	0.1	0.0
1*H*-TA4	22.45	22.05	23.52	0.0	0.0
2*H*-TA4	26.50	26.74	27.56	0.0	0.0
transition states	ΔE	ΔE_{ZPE}	ΔG	ν_i	
TS1	239.50	222.29	222.64	1728i	
TS2	9.38	0.85	15.32	29i	

[a] A_{342}, calculated gas phase abundance at 342 K. A_w, abundance estimated from the experimental band intensities weighted by the theoretically calculated IR intensities.

TS1 and TS2 joining the most stable minima are included in this table whereas the corresponding B3LYP/6-311++G(2d,2p) potential energy diagram is presented in Figure 2.

3.2. Population of the TA Species. Assuming that the equilibrium between the TA minima is achieved in the gas phase, the predicted gas phase population at the deposition temperature 342 K of the 1*H*-TA1 form equals 75.2% whereas the population of the next two most energetically favorable species (2*H*-TA1, 2*H*-TA2) equals 15.5 and 8.0%, respectively. The high energy barrier of 222 kJ mol^{-1} predicted for the unimolecular 1*H*-TA1 → 2H-TA1 tautomerization (see Figure 2) suggests that the thermodynamic equilibrium between tautomers 1*H*-TA1 and 2*H*-TA1 may not be established in the gas phase at the deposition temperature. As it will be shown later, all three most stable 1*H*-TA1, 2*H*-TA1, and 2*H*-TA2 species are present in argon matrices at 15 K however with population different than that mentioned above. Similar situation was already reported for several other molecules.[21,43−45] An explanation for this phenomenon was given by Yang and Rodgers for the case of cytosine.[46] The appearance in the gas phase of some tautomers, in spite of the large value of the energy barrier between them, was explained by a significant lowering of the tautomerization barriers in hydrogen bonded aggregates present in the gas phase before condensation as compared to the unimolecular tautomerization. The same mechanism is expected to work in the case of the TA species. A real population of each TA form in the matrices were thus estimated empirically on the basis of the experimental integrated band intensities weighted by the theoretically calculated IR intensities. These values were found to be: 58.9, 38.5, and 2.6% for 1*H*-TA1, 2*H*-TA1, and 2*H*-TA2, respectively (see Table 2), and as it will be shown further they reflect very well the population of the species in the TA/Ar matrices.

3.3. IR Spectrum of the Matrix Isolated TA and Its Comparison with the Theoretical Predictions. The infrared spectrum of TA isolated in solid argon at 15 K (11 K for measurements) is presented in Figure 3. This spectrum is compared with the sum spectrum theoretically predicted for the 1*H*-TA1, 2*H*-TA1, and 2*H*-TA2 species scaled by their abundances estimated according to the procedure described above. The majority of TA is present in the 1*H*-TA1 or 2*H*-TA1 forms, whereas 2*H*-TA2 is hardly noticeable. The infrared spectrum of TA in solid argon consists of two groups of bands: one associated with the vibrational modes of carboxylic group and the second related to the tetrazole ring. The whole set of the frequencies and intensities of the most stable TA species together with their assignment is provided as Table S1 in the Supporting Information. As seen from Figure 3, the bands due to the 1*H*-TA1 tautomer can be easily distinguish from those associated with the 2*H*-TA1 form. The bands resulting from 2H-TA1 exhibit in many regions splitting due to its occupancy of different matrix sites. It is worth noting that bands originating from the 1*H*-TA1 tautomer do not show site splitting effect. A probably explanation is presence of the intramolecular hydrogen bond in 1*H*-TA1 that increases rigidity of the molecular structure decreasing its susceptibility on the environment changes.

3.4. Results of Thermal Decomposition of TA Species. *3.4.1. Identification of the Decomposition Products.* From the very beginning of our experiment, it became clear that preparation of the matrices containing TA was not an easy task. We encountered a high propensity of the compound for thermal decomposition. It was found that traces of water present in the solid sample induced a partial decomposition of the compound during even mild heating. It was interesting to follow these reactions with the aim to compare them with the results of the UV photolytic decomposition observed in matrices (described in the following chapter). Figure 4 shows the representative portions of the spectrum of the products appearing in argon matrices after decomposition of the TA sample at ca. 350 K (upper panel, red trace). For comparison, the spectrum of the TA species isolated in solid argon obtained at conditions that avoided the thermal decomposition of the sample is also presented (upper panel, black trace). Analysis of these spectra indicates that heating of the TA sample with the trace water contamination induces, in addition to the bands characteristic of the 1*H*-TA1 and 2*H*-TA tautomers, appearance of new, intense bands in many regions of the spectra.

All new absorptions but two were found to be a spectral signature of 5-methyltetrazole (MT) that appeared in the matrix due to the decarboxylation of gaseous TA prior to the deposition. In order to confirm the suggested way of the TA decomposition, a spectrum of 5-methyltetrazole itself isolated in an argon matrix is shown in the bottom panel of Figure 4 (blue trace).[45] The MT molecule may exist in two tautomeric forms and according to the theoretical calculations the 2*H*-MT tautomer is predicted to be the predominant form with the

dx.doi.org/10.1021/jp5001804 | J. Phys. Chem. A 2014, 118, 2072−2082

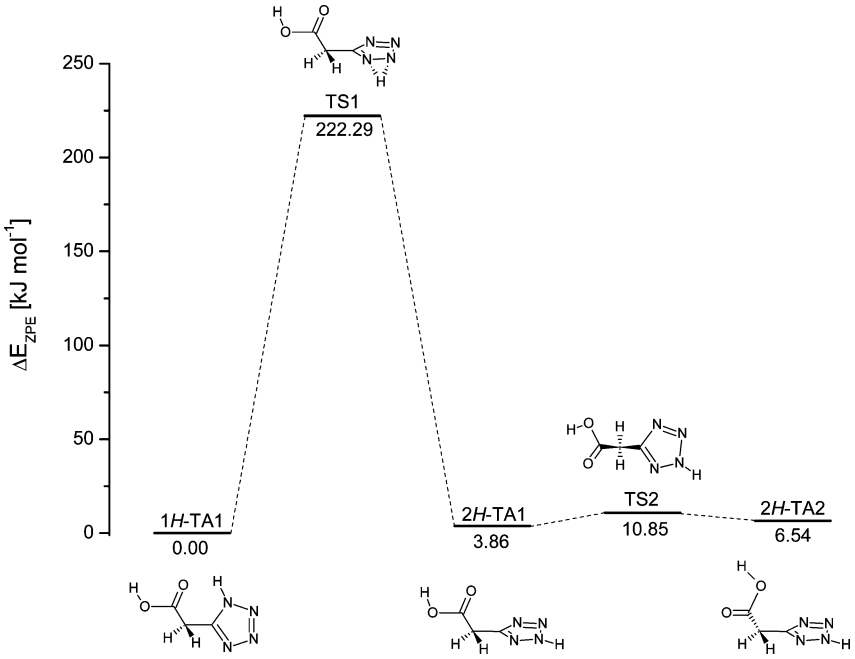

Figure 2. B3LYP/6-311++G(2d,2p) ZPE corrected potential energy diagram for isomerizations of three most stable TA structures.

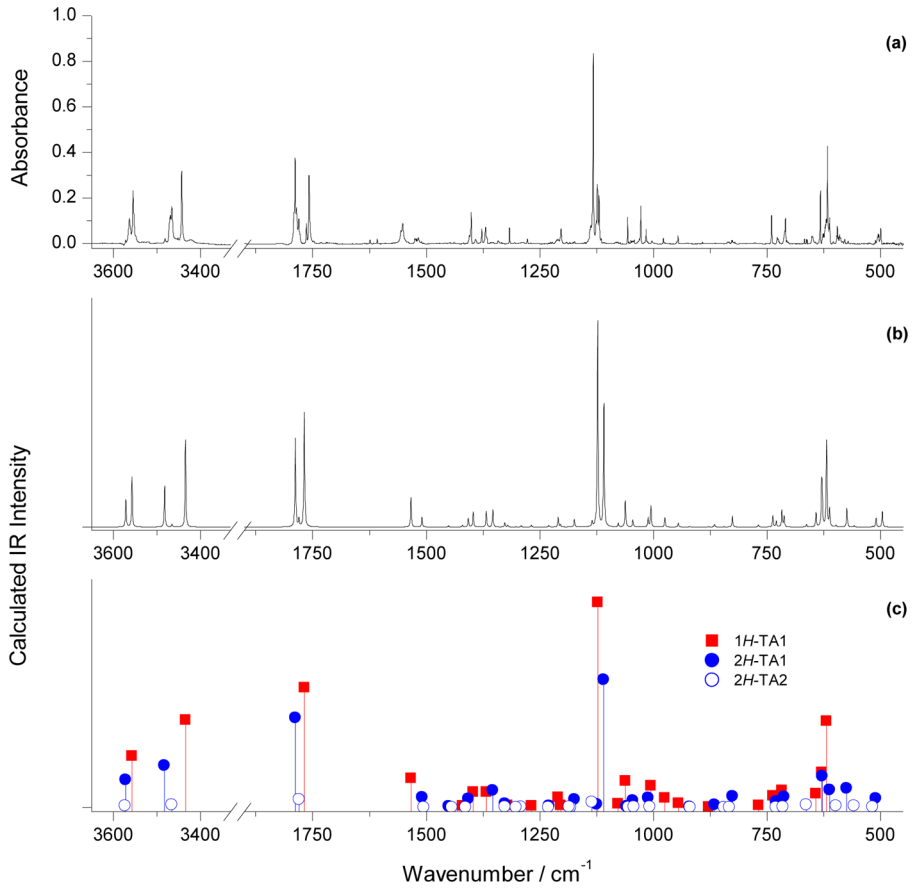

Figure 3. Infrared spectra of TA: (a) experimental spectrum of TA isolated in an argon matrix deposited at 15K and measured at 11K; (b) simulated sum spectrum obtained by adding the B3LYP/6-311++G(2d,2p) anharmonic spectra of 1*H*-TA1, 2-TA1, and 2*H*-TA2 isomers taken with the abundances estimated from band intensities weighted by the theoretically calculated IR intensities. The theoretical spectrum was created using Lorentzian functions with the fwhm = 2 cm^{-1}; (c) theoretical anharmonic spectra of the 1*H*-TA1, 2*H*-TA1, and 2*H*-TA2 isomers.

estimated populations ca. 95% at room temperature.[45,47] The experimental spectra obtained after decarboxylation of TA confirm that the majority of 5-methyltetrazole is present in the 2*H* form that is evident for example in the ν NH stretching mode of MT (3490−3430 cm^{-1} region in Figure 4). In addition to the bands due to MT, new absorptions appearing after TA

dx.doi.org/10.1021/jp5001804 | J. Phys. Chem. A 2014, 118, 2072−2082

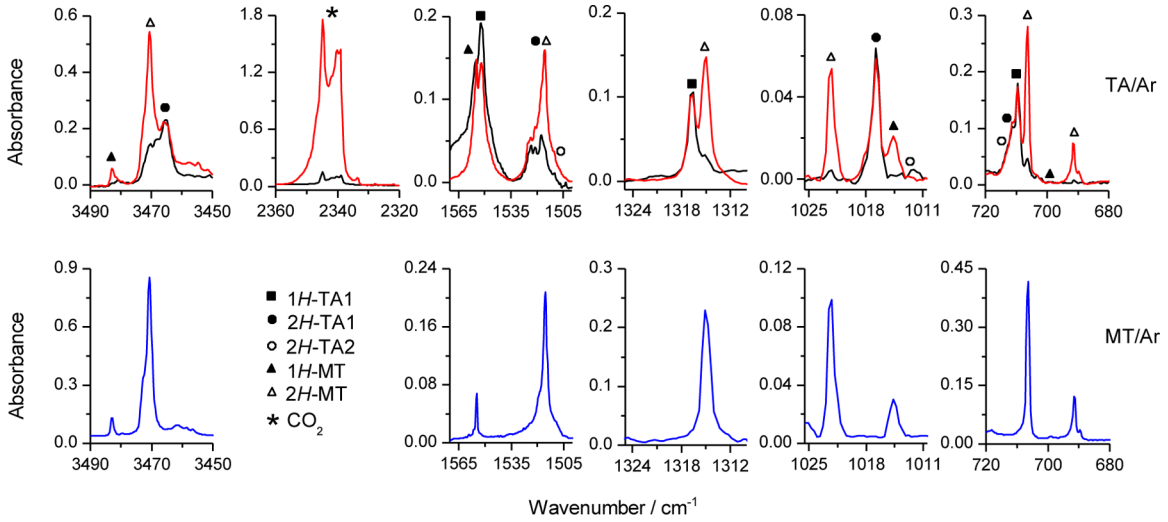

Figure 4. Selected regions of the infrared spectrum of TA/Ar matrix obtained after decomposition of the TA sample at ca. 350 K (upper panel, red traces). For comparison, the spectrum of the TA species isolated in solid argon obtained at conditions that avoided the thermal decomposition of the sample is also presented (upper panel, black traces); the infrared spectrum of MT/Ar matrix (bottom panel, blue traces).

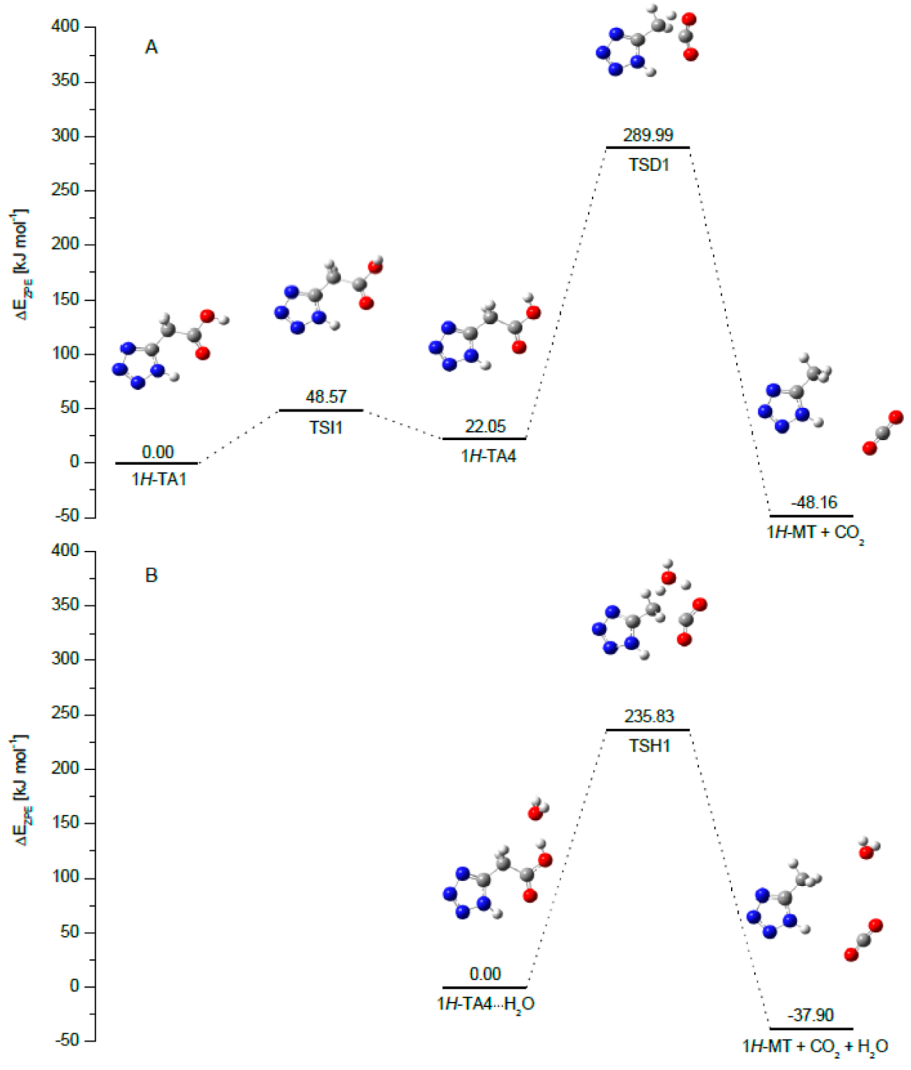

Figure 5. B3LYP/6-311++G(2d,2p) energy diagram for the decarboxylation of 1*H*-TA1 tautomer proceeding without (A) and with (B) water molecule presence. The energetics of the final products was calculated under the assumption that the nascent CO_2 (and H_2O) molecules had departed.

dx.doi.org/10.1021/jp5001804 | J. Phys. Chem. A 2014, 118, 2072−2082

decomposition are detected in the 2360−2340 and 670−660 cm^{-1} regions due to the asymmetric stretching and bending modes of the CO_2 molecule. The obtained results show that, at the conditions of our experiment, a decarboxylation is the only process observed for thermal decomposition of TA (in the presence of water traces) at our conditions of experiment and no further reactions, observed at higher temperatures by Pinto et al.[47] were detected.

3.4.2. TA Decomposition and Water Assisted TA Decomposition Pathways. To gain an insight into the decomposition pathway detected experimentally, the B3LYP/6-311++G(2d,2p) calculations were carried out on the mechanism of the reaction. The potential energy diagrams of the 1*H*-TA1 and 2*H*-TA1 decarboxylation processes are shown in Figures 5A and S2A (Supporting Information), respectively. Analysis of these data shows that rotation of the OH group of the carboxylic group changing cis conformation into the trans form of the precursor molecule is the first step necessary for the TA decarboxylation to proceed. Thus, 1*H*-TA1 and 2*H*-TA1 are transformed into 1*H*-TA4 and 2*H*-TA4 through the TSI1 and TSI2 transition states, respectively.

The ZPE corrected energy barriers estimated for these processes are equal to 48.57 and 47.74 kJ mol^{-1} and are consistent with those reported for such isomerization of other carboxylic acids.[48−50] Next, the decarboxylation reaction takes place through the TSD1 and TSD2 transition states with the energy barriers of 267.94 and 260.21 kJ mol^{-1}, respectively, for 1*H*-TA4 and 2*H*-TA4. The energy barriers toward decarboxylation for other carboxylic acids or amino acids were reported to be within the range 170−290 kJ mol^{-1}.[51−58]

The intrinsic reaction coordinate (IRC) analysis performed for TSD1 and TSD2 indicates that during the decarboxylation process a shift of the carboxylic hydrogen to the C7 carbon atom is accompanied by a gradual elongation of the C7−C10 bond and a decrease of the C10O12H13 angle. In further steps of the reaction, the O═C═O angle increases up to 180° in the CO_2 molecule. According to the calculations, the exothermicity of the overall process is equal to 48.16 and 59.37 kJ mol^{-1} for 1*H*-TA1 and 2*H*-TA1, respectively.

To consider a possible mechanism of the TA decarboxylation aided by water molecule, we calculated an energy barrier for this process in the 1:1 1*H*-TA4···H_2O and 2*H*-TA4···H_2O hydrogen bonded complexes. The relevant potential energy diagrams for the 1*H*-TA4···H_2O and 2*H*-TA4···H_2O species are shown in Figure 5B and Figure S2B (Supporting Information). The decarboxylation proceeds through the TSH1 and TSH2 transition states, respectively. The presence of the water molecule lowers the energy barrier for decarboxylation reaction by 32.11 and 26.58 kJ mol^{-1} (after zero-point vibrational correction) for 1*H*-TA4···H_2O and 2*H*-TA4···H_2O, respectively comparing to the corresponding processes without water participation. These values are within the range of the literature data. It was shown that in the case where water is available and forms a complex with the acid, it lowers the energy for elimination (also decarboxylation) reaction by one quantuum of an O−H stretch[57,59,60] and our results fit well to this value.

3.5. Results of the UV Irradiation of the TA/Ar Matrices. *3.5.1. Tautomer-Selective Photochemistry.* The experimental spectrum of the TA/Ar sample recorded directly before irradiation experiments showed that three 1*H*-TA1, 2*H*-TA1, and 2*H*-TA2 isomers were present in the matrix. Such matrices were subjected to both broad-band (high pressure xenon lamp) and narrow-band (OPO) irradiations. After each irradiation, an infrared spectrum of the matrix was taken to monitor possible transformations of the precursor molecules. The obtained results will be discussed in the following paragraphs.

In the course of the performed photolysis experiments, an interesting phenomenon was detected. UV irradiation of the TA/Ar matrix with a high-pressure Xe lamp (with the optical filter $\lambda > 280$ nm) led to consumption of the 2*H*-TA1 and 2*H*-TA2 species whereas 1*H*-TA1 remained intact. Using full output of the xenon lamp resulted in the 1*H*-TA1 tautomer destruction as well. The same effect was also evident when narrow-band radiation from the tunable OPO laser system was applied. The laser irradiation with $\lambda \leq 244$ nm led to destruction of both 2*H*-TA1 and 2*H*-TA2 species, whereas irradiation with $\lambda \leq 235$ nm resulted in depletion of the 1*H*-TA1 tautomer. The observed phenomenon of the tautomer-selective photochemistry of TA can be understood on the basis of the results of the performed time-dependent density functional theory (TD-DFT) calculations. Indeed, the estimated $S_0 \rightarrow S_1$ and $S_0 \rightarrow S_2$ energy gaps for 1*H*-TA1 differ by several nanometers from those calculated for 2*H*-TA1 (see Table S2 in the Supporting Information). Such differences justify different threshold energies necessary to start the photolysis of the 1*H*-TA1 and 2*H*-TA1 (2*H*-TA2) species. Figure 6 presents plots of the normalized integrated absorbance

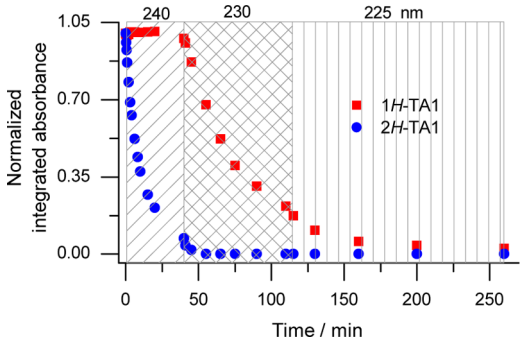

Figure 6. Plots of the normalized integrated absorbance versus narrow-band irradiation time observed for the νNH bands of 1*H*-TA1 (red solid squares) and 2*H*-TA1 (blue solid circles). Normalization of the integrated absorbance was performed relative to the intensity values in the initial spectrum. The wavelength used is specified at the top of the figure.

changes versus the narrow-band irradiation time observed for the νNH bands of the 1*H*-TA1 and 2*H*-TA1 species. Similar effect was earlier observed for other tetrazole containing compounds isolated in solid argon, namely 5-(1*H*-tetrazol-1-yl)-1,2,4-triazole and 5-methyltetrazole.[21,45]

3.5.2. Photolysis Using High Pressure Xenon Lamp. Irradiation of the TA/Ar matrices deposited at 15 K (measurement at 11 K) using high pressure xenon lamp (with the optical filter $\lambda > 280$ nm) led to depletion of the 2*H*-TA species and, simultaneously, to appearance of a number of new bands due to photoproducts. These changes are shown in Figure 7 where representative portions of the spectrum obtained after deposition (black traces) are compared to those taken after 120 min of the $\lambda > 280$ nm irradiation (red traces). Upon further irradiation of the matrix with full output of the lamp, the bands due to the remaining amount of 2*H*-TA species disappeared and those of 1*H*-TA1 strongly decreased. Parallel with the 1*H*-TA1 depletion, another set of bands grew

dx.doi.org/10.1021/jp5001804 | J. Phys. Chem. A 2014, 118, 2072−2082

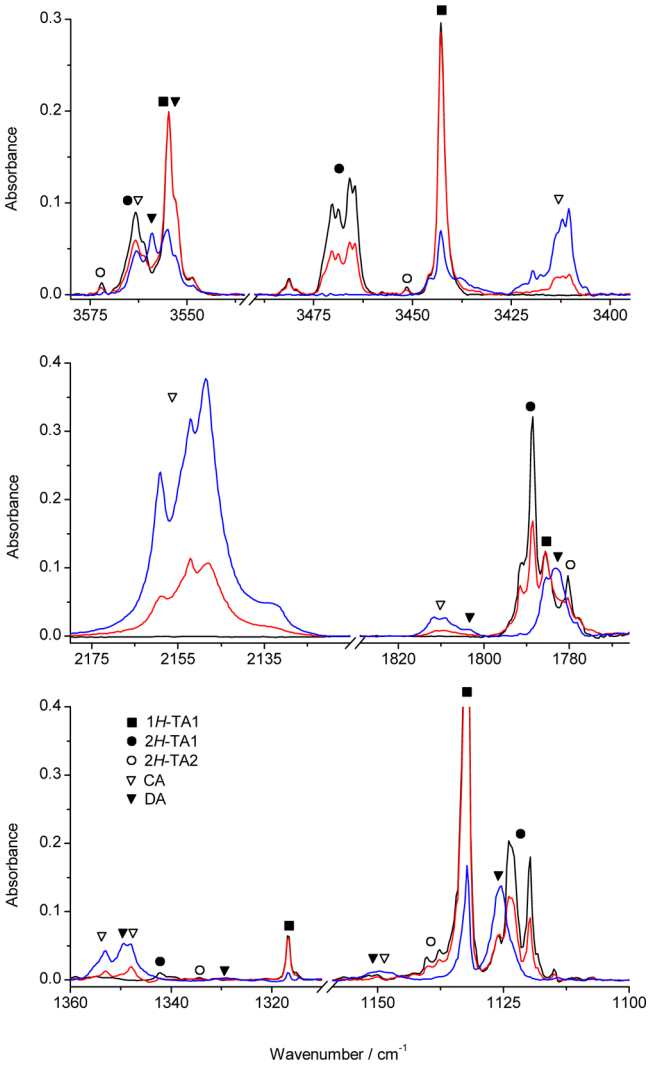

Figure 7. Selected regions of the TA/Ar experimental spectra obtained for freshly deposited matrix (black traces), the same matrix taken after 120 min of the $\lambda > 280$ nm irradiation by Xe lamp (red traces) and after further 120 min of irradiation with full output of Xe lamp (blue traces).

in the spectrum (blue traces in Figure 7). Relatively broad absorptions appearing upon photolysis were found in many spectral regions at frequencies similar to those due to the precursor molecules. In particular, closer inspection of the νOH region revealed that the band situated at 3563 cm^{-1} due to the 2*H*-TA1 species did not vanish completely in the spectrum after photolysis with full output of the lamp whereas all other absorptions of 2*H*-TA1 disappeared. Apparently, another νOH absorption due to a photoproduct grew in this region. Two other bands appeared in this region at 3559 and 3555 cm^{-1}, with the first one clearly seen and the second one overlapping with the νOH absorption of 1*H*-TA1. Table 3 gathered selected experimental frequencies of the bands arising from the photolysis compared to the corresponding theoretical predictions. The complete list of frequencies of the photoproducts is collected in Table S3 in the Supporting Information.

Comparison of the frequencies of the bands appearing in the spectra upon photolysis with those calculated for the possible photoproducts indicates formation of two main photoproducts, both appearing as a result of the tetrazole ring cleavage. First of them is carbodiimidylacetic acid. The obtained result is not unexpected since it was shown that 1,5-disubstituted tetrazoles were useful precursors of carbodiimides.[17,23] However, to the best of our knowledge carbodiimide bearing the COOH group has not been described before. Here, carbodiimidylacetic acid was identified on the basis of 18 absorptions, many of them broad and consisting of several subbands. The key bands that allowed for the identification are those observed at 3563, ca. 3415, 2150, and 1810 cm^{-1} characteristic of the stretching νOH, νNH, ν_{as}NCN, and νC═O modes, respectively. According to the calculations two different conformers are expected for the carbodiimidylacetic differing in the position of the NCNH group relative to the carboxylic group. These structures (denoted as CA species) are shown in Table 3 together with their calculated frequencies and intensities.

The second photoproduct, although its weak bands were also seen after the $\lambda > 280$ nm irradiation, was clearly observed in the spectra upon photolysis of the 1*H*-TA1 species. It is characterized by a set of fourteen absorptions, most of which are split into two or three components (see Tables 3 and S3 (Supporting Information)). By comparison with the results of the performed calculations, this photoproduct was identified as unknown before (1*H*-diaziren-3-yl)acetic acid (denoted as DA). Several 1,3-disubstituted 1*H*-diazirines have already been described;[18,20,61] however, much less data is available on the 1*H*-diazirines with unsubstituted N−H group.[62] According to the calculations vibrations originating from the carboxylic group are expected to be much stronger than those assigned to the diazirine moiety. Indeed, such spectral picture was observed experimentally. The identification was based on the features characteristic of the COOH and diazirine groups. Intense bands at ca. 3557, 1784, and 1135 cm^{-1} are assigned to the νOH, νC═O, and νC−O modes, respectively. In turn, weak absorptions at ca. 3240, 1803, and 1322 cm^{-1} due to the νNH, νC═N, and δNH modes originate from the diazirine subunit. Similarly as for the carbodiimidylacetic acid (CA), there are several conformers possible for the (1*H*-diaziren-3-yl)acetic acid. They differ in the relative arrangement of the diazirine and carboxylic groups. Two of such DA structures are presented in Table 3 together with the calculated frequencies and intensities.

3.5.3. Photolysis Using Tunable Narrow-Band UV Source. A series of irradiations of the TA/Ar matrices was carried out with narrow-band radiation in the 250−225 nm range. Generally, the same photoproducts as those detected upon the broad-band irradiation were observed when the laser source was applied. However, the bands originating from the CA and DA photoproducts whose intensity was increasing initially upon irradiation at 240 nm stopped growing when the shorter wavelengths (235−225 nm) were used. Simultaneously, a number of additional absorptions appeared indicating that some secondary processes have been taking place in the matrices. Figure 8 presents selected regions of the TA/Ar spectra after 90 min of laser irradiation compared to the spectra of TA/Ar obtained directly after deposition. The most intense secondary products bands are situated at ca. 3600, 3295, 2344, 2135, 736, and 660 cm^{-1}. Figure 9 shows a plot of the normalized integrated absorbance of the CA band at ca.1810 cm^{-1} (νC═O) and of the product band at 3295 cm^{-1} (νCH) versus time of irradiation. The observed set of absorptions suggests that the destruction of the observed photoproducts CA and probably also DA took place accompanied with the formation of the CO_2, HCN (or HNC)[45] species. Since these

dx.doi.org/10.1021/jp5001804 | J. Phys. Chem. A 2014, 118, 2072−2082

Table 3. Selected Experimental and B3LYP/6-311++G(2d,2p) Calculated (scaled) Frequencies[a] and Intensities of the Photoproducts Observed after Photolysis of TA/Ar Matrix

Calculated				Ar (15 K)	Approximate Description[b]
ν	I	ν	I	ν	
carbodiimidylacetic acid (CA)					
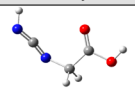		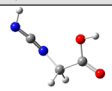			
3572	77	3570	79	3563	νOH
3415	88	3413	83	3420, 3412	νNH
2170	951	2175	990	2159, 2152, 2148	ν_{as}NCN
1781	206	1772	360	1812, 1809	νC=O
1291	16	1331	37	1348	δOH + ωCH_2
1124	315	1150	189	1147	νCO + δOH + ωCH_2
918	234	917	233	880, 869, 863, 855, 851	δNH
633	85	644	47	641	γOH + δCH_2 + γOCO
562	41	556	43	549	γNH + τNCNC + δOCO + δCCO
(1*H*-diaziren-3-yl)acetic acid (DA)					
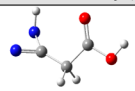		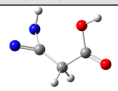			
3567	88	3563	89	3559, 3555	νOH
3236	4	3234	2	3240, 3236, 3233	νNH
1849	31	1844	9	1803	νC=N
1777	276	1783	435	1783, 1785	νC=O
1365	83	1351	15	1349, 1329	δOH + ωCH_2 + νCC + νCO + δOCO + δCCO
1346	6	1323	30	1322, 1315	δNH + νCN
1127	304	1155	252	1126, 1149	νCO + δOH + ωCH_2
1010	83	1010	47	960, 954, 949	γNH
646	55	667	96	642, 660	γOH + γOCO + δOCO + δCCO
638	68	617	41	624, 602	γOH + δOCO + δCCO
nitriliminylacetic acid (NA)					
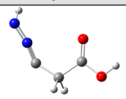		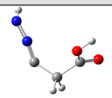			
3569	74	3571	75	3561	νOH
3259	14	3256	13	n.o.	νNH
2134	486	2137	434	2107, 2103, 2089, 2083	ν_{as}NNC
1785	199	1773	392	1775	νC=O
1282	38	1298	13	1292	δOH + ωCH_2 + δNH + δOCO
1265	139	1257	230	1255, 1247	δNH + νNN + δCH_2 + δOH
1111	335	1128	168	1117	ωCH_2 + νCO + δOH + δOCO
637	88	604	157	620	γOH + δCH_2 + γNH
581	86	577	91	565	γNH + γOH + τNNCC + δCH_2

[a]Scaling factors equal to 0.95 and 0.98 above and below 2800 cm^{-1}, respectively. [b]Abbreviations: ν, bond stretching; δ, bending; deformation in plane, γ, out-of-plane bending; τ, torsion; r, rocking; ω, wagging; t, twisting.

products are expected to be isolated in the same matrix cage together with the N_2 molecule originating from the tetrazole ring cleavage, different molecular complexes may be formed resulting in the observed spectral pattern. It is worth noting that the calculated energy barriers for the HCN ↔ HNC transformations are equal to 183.48 and 126.06 kJ mol^{-1} for the forward and reverse reactions, respectively[45] Thus, such conversions are possible under the applied irradiation conditions as well.

It is worth mentioning that, at the very early stage of narrow-band irradiation, a set of weak absorptions appeared in several regions of the spectra that increased initially and then disappeared at longer time of photolysis. These bands are listed in Table 3 and in Table S3 in the Supporting Information and are tentatively assigned to the nitriliminylacetic acid (NA) on the basis of both theoretical predictions and our earlier observation of the analogous species with the CNNH moiety reported as a result of the UV photolysis of 5-methyltetrazole.[45]

Summary of the UV Photolysis Pathways. The proposed pathways resulting from the UV photolysis of the 1*H*-TA1 and 2*H*-TA1 species in solid argon are presented in Figure 10. For clarity, transformations of the least abundant 2*H*-TA2 form are

dx.doi.org/10.1021/jp5001804 | J. Phys. Chem. A 2014, 118, 2072−2082

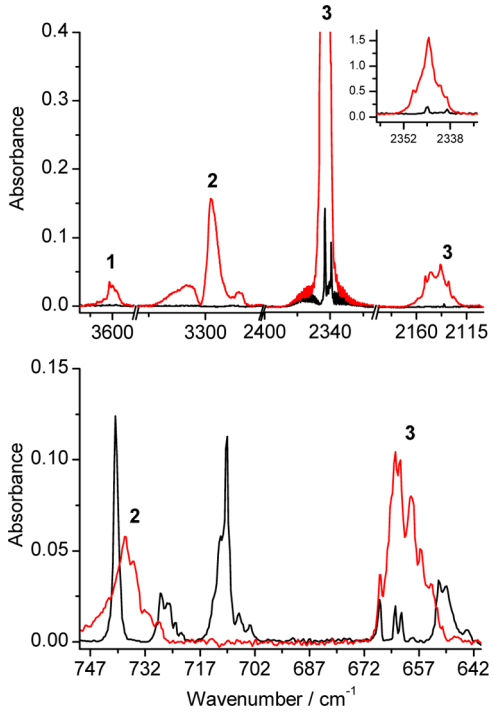

Figure 8. Selected regions of the TA/Ar experimental obtained for freshly deposited matrix (black traces) and the same matrix after 90 min of laser irradiation at 225 nm (red traces). 1, 2, and 3 denote HNC, HCN, and CO_2 and their complexes, respectively.

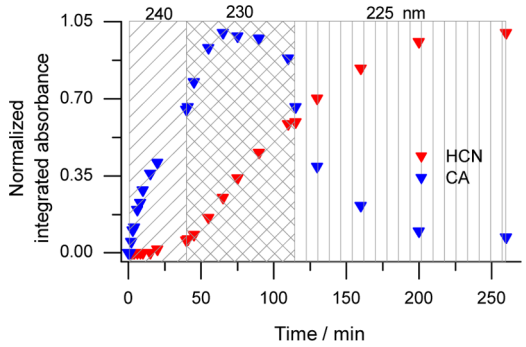

Figure 9. Plots of the normalized integrated absorbance of the CA band (ca. 1810 cm^{-1}, νC═O) and of one of the product bands (3295 cm^{-1}, νCH) versus time of irradiation at 225 nm.

not shown in this figure, since they are expected to proceed in a similar way as those shown for 2*H*-TA1.

The reactions proceeding upon UV irradiation of the TA/Ar matrices involving the tetrazole ring cleavage follow the general trend found for other 5-substituted tetrazoles.[23,24,45] Elimination of the N_2 molecule leads, in the first stage, to the nitrene-type intermediate in the case of the 1*H*-TA1 tautomer whereas nitriliminyl carboxylic acid (detected only at the beginning of the laser irradiation) is formed when 2*H*-TA is involved. Then, in both cases, a cyclic compound of the diazirine-type is expected to be formed. Such cyclic species usually escape detection being quickly transformed to the corresponding carbodiimides (CA). In the present study, we do observe (1*H*-diaziren-3-yl)acetic acid (DA), most probably in two conformational forms.

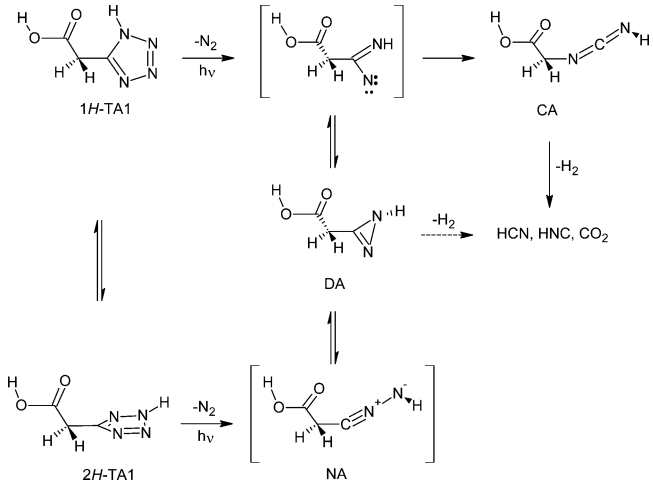

Figure 10. Proposed photolysis pathways resulting from irradiation of the TA/Ar matrices.

4. CONCLUSIONS

In agreement with the results of the B3LYP/6-311++G(2d,2p) calculations, three isomers of (tetrazol-5-yl)acetic acid (TA) were identified in low temperature argon matrices. The most stable and the most abundant is the *1H* tautomer (1*H*-TA1) characterized by the intramolecular N−H···O hydrogen bond between the tetrazole ring N−H group and the carbonyl group. Next two most stable TA species are *2H* tautomers (2*H*-TA1, 2*H*-TA2) with almost perpendicular arrangement of the ring relative to the carboxylic group plane. They are by 3.86 and 6.54 kJ mol^{-1} less stable than 1*H*-TA1. TA was found to decompose easily while heated to moderate temperature at the presence of water traces. Experimentally, the process was followed by FTIR spectroscopy and products of such thermal decomposition, 5-methyltetrazole and carbon dioxide, were detected in argon matrices. The mechanism of the decarboxylation process was explained on the basis of the results of the performed calculations. The TA decarboxylation as well as the corresponding water assisted process were described in detail using B3LYP/6-311++G(2d,2p) method. It was shown that the presence of water molecule lowered the energy barrier for decarboxylation by ca. 30 kJ mol^{-1} comparing to the corresponding process without water participation.

The UV photolysis of the TA/Ar matrices with the broad-band source led to carbodiimidylacetic acid (CA) and (1*H*-diaziren-3-yl)acetic acid (DA) as main photoproducts, both arising from the tetrazole ring cleavage. To the best of our knowledge, neither of these species have ever been described before. When narrow-band irradiation was applied, secondary reactions took place in the TA/Ar matrices as well. Several additional species originating from decomposition of the main products were identified in the spectra, in particular HCN, HNC, CO_2, and their molecular complexes.

■ ASSOCIATED CONTENT

Supporting Information

Frequencies and intensities of the most stable TA species together with their assignment (Table S1), TD-DFT calculated values of the energies of the electronic excitations for the 1*H*-TA1, 2*H*-TA1, and 2*H*-TA2 species (Table S2), complete list of the photoproducts frequencies and intensities (Table S3), the B3LYP/6-311++G(2d,2p) optimized geometry of the TA

dx.doi.org/10.1021/jp5001804 | J. Phys. Chem. A 2014, 118, 2072−2082

species (Figure S1), and the B3LYP/6-311++G(2d,2p) energy diagram for the decarboxylation of 2*H*-TA1 (Figure S2). This material is available free of charge via the Internet at http://pubs.acs.org.

AUTHOR INFORMATION

Corresponding Author

*E-mail: maria.wierzejewska@chem.uni.wroc.pl. Tel.: +48-71-375-7332. Fax: +48-71-328-2348.

Notes

The authors declare no competing financial interest.

ACKNOWLEDGMENTS

A grant of computer time from the Wrocław Center for Networking and Supercomputing is gratefully acknowledged.

REFERENCES

(1) Joo, Y-H; Shreeve, J. M. High-Density Energetic Mono- or Bis(oxy)-5-nitroiminotetrazoles. *Angew. Chem., Int. Ed.* **2010**, *49*, 7320−7323.

(2) Zhang, Q.; Shreeve, J. M. Growing Catenated Nitrogen Atom Chains. *Angew. Chem., Int. Ed.* **2013**, *52*, 8792−8794.

(3) Zhang, Q.; Zhang, J.; Parrish, D. A.; Shreeve, J. M. Energetic N-trinitroethyl-substituted Mono-, Di-, and Triaminotetrazoles. *Chem.—Eur. J.* **2013**, *19*, 11000−11006.

(4) Dippold, A. A.; Izsák, D.; Klapötke, T. M. A Study of 5-(1,2,4-Triazol-*C*-yl)tetrazol-1-ols: Combining the Benefits of Different Heterocycles for the Design of Energetic Materials. *Chem.—Eur. J.* **2013**, *19*, 12042−12051.

(5) Fischer, D.; Klapötke, T. M.; Piercey, D. G.; Stierstorfer, J. Synthesis of 5-Aminotetrazole-1-N-oxide and Its Azo Derivative: A Key Step on the Development of New Energetic Materials. *Chem.—Eur. J.* **2013**, *19*, 4602−4613.

(6) Hassan, N.; Stelzl, J.; Weinberger, P.; Molnar, G.; Bousseksou, A.; Kubel, F.; Mereiter, K.; Boca, R.; Linert, W. Spectroscopic, Structural and Magnetic Investigations of Iron(II) Complexes Based on 1-Isopropyl- and 1-Isobutyl-substituted Tetrazole Ligands. *Inorg. Chim. Acta* **2013**, *396*, 92−100.

(7) Białońska, A.; Bronisz, R.; Kusz, J.; Zubko, M. Two-step Spin Trasition in an Iron(II) Coordination Network Based on Flexible Bitopic Ligand 1-(Tetrazol-1-yl)-3-(1,2,3-triazol-1-1yl)propane. *Eur. J. Inorg. Chem.* **2013**, 884−893.

(8) Herr, R. J. 5-Substituted-1*H*-tetrazoles as Carboxylic Acid Isosteres: Medicinal Chemistry and Synthetic Methods. *Bioorg. Med. Chem.* **2002**, *10*, 3379−3393.

(9) Myznikov, L. V.; Hrabalek, A.; Koldobskii, G. I. Drugs in the Tetrazole Series. *Chem. Heterocycl. Compd.* **2007**, *43*, 1−9.

(10) Matta, C. F.; Arabi, A. A.; Weaver, D. F. The Bioisosteric Similarity of the Tetrazole and Carboxylate Anions: Clues from the Topologies of the Electrostatic Potential and of the Electron Density. *Eur. J. Med. Chem.* **2010**, *45*, 1868−1872.

(11) Singh, H.; Chawla, A. S.; Kapoor, V. K.; Paul, D.; Malhotra, R. K. Medicinal Chemistry of Tetrazoles. *Prog. Med. Chem.* **1980**, *17*, 151.

(12) May, B. C. H.; Abell, A. D. Methylene Tetrazole-Based Peptidomimetics: Synthesis and Inhibition of HIV Protease. *J. Chem. Soc., Perkin Trans. 1* **2002**, *1*, 172−178.

(13) Bekircan, O.; Bektas, H. Synthesis of New Bis-1,2,4-triazole Derivatives. *Molecules* **2006**, *11*, 469−477.

(14) Rostom, S. A. F.; Ashour, H. M. A.; Abd El Razik, H. A.; Abd El Fattah, H.; El-Din, N. N. Azole Antimicrobial Pharmacophore-based Tetrazoles: Synthesis and Biological Evaluation as Potential Antimicrobial and Anticonvulsant Agents. *Bioorg. Med. Chem.* **2009**, *17*, 2410−2422.

(15) Allen, F. H.; Groom, C. R.; Liebeschuetz, J. W.; Bardwell, D. A.; Olsson, T. S. G.; Wood, P. A. The Hydrogen Bond Environments of 1H-Tetrazole and Tetrazolate Rings: The Structural Basis for Tetrazole-carboxylic Acid Bioisosterism. *J. Chem. Inf. Model.* **2012**, *52*, 857−866.

(16) Maier, G.; Eckert, J.; Bothur, A.; Reisenauer, H. P.; Schmidt, C. Photochemical Fragmentation of Unsubstituted Tetrazole, 1,2,3-Triazole, and 1,2,4-Triazole. First Matrix-spectroscopic Identification of Nitrilimine HCNNH. *Liebigs Ann.* **1996**, 1041−1053.

(17) Yranzo, G. I.; Elguero, J.; Flammang, R.; Wentrup, C. Formation of Cumulenes, Triple-bonded, and Related Compounds by Flash Vacuum Thermolysis of Five-membered Heterocycles. *Eur. J. Org. Chem.* **2001**, 2209−2220.

(18) Gómez-Zavaglia, A.; Reva, I. D.; Frija, L. M. T.; Cristiano, M. L. S.; Fausto, R. Molecular Structure, Vibrational Spectra and Photochemistry of 2-Methyl-2*H*-tetrazol-5-amine in Solid Argon. *J. Phys. Chem. A* **2005**, *109*, 7967−7976.

(19) Gómez-Zavaglia, A.; Reva, I. D.; Frija, L. M. T.; Cristiano, M. L. S.; Fausto, R. Infrared Spectrum and UV-induced Photochemistry of Matrix-isolated 5-Methoxy-1-phenyl-1*H*-tetrazole. *J. Photochem. Photobiol. A* **2006**, *180*, 175−183.

(20) Frija, L. M. T.; Reva, I. D.; Gómez-Zavaglia, A.; Cristiano, M. L. S.; Fausto, R. Photochemistry and Vibrational Spectra of Matrix-isolated 5-Ethoxy-1-phenyl-1*H*-tetrazole. *J. Phys. Chem. A* **2007**, *111*, 2879−2888.

(21) Pagacz-Kostrzewa, M.; Reva, I. D.; Bronisz, R.; Giuliano, B. M.; Fausto, R.; Wierzejewska, M. Conformational Behavior and Tautomer Selective Photochemistry in Low Temperature Matrices: the Case of 5-(1*H*-Tetrazol-1-yl)-1,2,4-triazole. *J. Phys. Chem. A* **2011**, *115*, 5693−5707.

(22) Pagacz-Kostrzewa, M.; Krupa, J.; Olbert-Majkut, A.; Podruczna, M.; Bronisz, R.; Wierzejewska, M. Conformational Properties and Photochemistry of Tetrazolylpyridines in Low Temperature Matrices. Spectroscopic Evidence for the Photochemical Carbon-To-Nitrogen Rearrangement. *Tetrahedron* **2011**, *67*, 8572−8582.

(23) Bégué, D.; Qiao, G. H.; Wentrup, C. Nitrile Imines: Matrix Isolation, IR Spectra, Structures, and Rearrangement to Carbodiimides. *J. Am. Chem. Soc.* **2012**, *134*, 5339−5350.

(24) Frija, L. M. T.; Cristiano, M. L. S.; Gómez-Zavaglia, A.; Reva, I.; Fausto, R. Genesis of Rare Molecules using Light-induced Reactions of Matrix-Isolated Tetrazoles. *J. Photochem. Photobiol. C* **2014**, *18*, 71−90.

(25) Alkorta, I.; Elguero, J. A Theoretical Study on the Tautomerism of C-Carboxylic and Methoxycarbonyl Substituted Azoles. *Struct. Chem.* **2005**, *16*, 507−514.

(26) Pagacz-Kostrzewa, M.; Jesariew, D.; Podruczna, M.; Wierzejewska, M. Infrared Spectra and X-ray Structure of (Tetrazol-5-yl)acetic Acid. *Spectrochim. Acta, Part A* **2013**, *108*, 229−235.

(27) Khriachtchev, L.; Maçôas, E. M. S.; Pettersson, M.; Räsänen, M. Conformational Memory in Photodissociation of Formic Acid. *J. Am. Chem. Soc.* **2002**, *124*, 10994−10995.

(28) Fausto, R.; Maçôas, E. M. S. Photochemical Reactivity of Matrix-Isolated Monomeric Carboxylic Acids. *J. Mol. Struct.* **2001**, *563*−*564*, 27−40.

(29) Isoniemi, E.; Khriachtchev, L.; Makkonen, M.; Räsänen, M. UV Photolysis Products of Propiolic Acid in Noble-Gas Solids. *J. Phys. Chem. A* **2006**, *110*, 11479−11487.

(30) Olbert-Majkut, A.; Ahokas, J.; Lundell, J.; Pettersson, M. Photolysis of HCOOH Monomer and Dimer in Solid Argon: Raman Characterization of *In Situ* Formed Molecular Complexes. *Phys. Chem. Chem. Phys.* **2010**, *12*, 7138−7147.

(31) Fausto, R.; Gómez-Zavaglia, A. Light Induced Reactions in Cryogenic Matrices. *Photochemistry* **2010**, *38*, 39−68.

(32) Nunes, C. M.; Reva, I.; Pinho e Melo, T. M. V. D.; Fausto, R.; Solomek, T.; Bally, T. The Pyrolysis of Isoxazole Revisited: A New Primary Product and the Pivotal Role of the Vinylnitrene. A Low-Temperature Matrix Isolation and Computational Study. *J. Am. Chem. Soc.* **2011**, *133*, 18911−18923.

(33) Scheer, A. M.; Mukarakate, C.; Robichaud, D. J.; Nimlos, M. R.; Ellison, G. B. Thermal Decomposition Mechanisms of the Methoxyphenols: Formation of Phenol, Cyclopentadienone, Vinylacetylene, and Acetylene. *J. Phys. Chem. A* **2011**, *115*, 13381−13389.

(34) Scheer, A. M.; Mukarakate, C.; Robichaud, D. J.; Nimlos, M. R.; Carstensen, H.-H.; Ellison, G. B. Unimolecular Thermal Decomposition of Phenol and d_5-Phenol: Direct Observation of Cyclopentadiene Formation via Cyclohexadienone. *J. Chem. Phys.* **2012**, *136*, 044309−1−11.
(35) Reva, I.; Nowak, M. J.; Lapinski, L.; Fausto, R. UV-Induced Amino → Imino Hydrogen-Atom Transfer in 1-Methylcytosine. *J. Phys. Chem. B* **2012**, *16*, 5703−5710.
(36) Frisch, M. J.; Trucks, G. W.; Schlegel, H. B.; Scuseria, G. E.; Robb, M. A.; Cheeseman, J. R.; Scalmani, G.; Barone, V.; Mennucci, B.; Petersson, G. A.; et al.. *Gaussian 09*, Revision D.01; Gaussian, Inc.: Wallingford, CT, 2009.
(37) Gonzalez, C.; Schlegel, H. B. An Improved Algorithm for Reaction Path Following. *J. Chem. Phys.* **1989**, *90*, 2154−2161.
(38) Gonzalez, C.; Schlegel, H. B. Reaction Path Following in Mass-Weighted Internal Coordinates. *J. Chem. Phys.* **1990**, *94*, 5523−5527.
(39) Bauernschmitt, R.; Ahlrichs, R. Treatment of Electronic Excitations Within the Adiabatic Approximation of Time Dependent Density Functional Theory. *Chem. Phys. Lett.* **1996**, *256*, 454−464.
(40) Stratmann, R. E.; Scuseria, G. E.; Frisch, M. J. An Efficient Implementation of Time-Dependent Density-Functional Theory for the Calculation of Excitation Energies of Large Molecules. *J. Chem. Phys.* **1998**, *109*, 8218−8224.
(41) Martin, J. M. L.; Van Alsenoy, C. *GAR2PED*, University of Antwerp: Antwerp, Belgium, 1995.
(42) Irikura, K. *Synspec*; National Institute of Standards and Technology: Gaithesburg, MD, 1995.
(43) Lapinski, L.; Nowak, M. J.; Reva, I.; Rostkowska, H.; Fausto, R. NIR-Laser-Induced Selective Rotamerization of Hydroxy Conformers of Cytosine. *Phys. Chem. Chem. Phys.* **2010**, *12*, 9615−9618.
(44) Pagacz-Kostrzewa, M.; Bronisz, R.; Wierzejewska, M. Theoretical and Matrix Isolation FTIR Studies of 3-Amino-1,2,4-triazole and Its Isomers. *Chem. Phys. Lett.* **2009**, *473*, 238−246.
(45) Pagacz-Kostrzewa, M.; Krupa, J.; Wierzejewska, M. Photochemical Transformations of 5-Methyltetrazole. Matrix Isolation FTIR and DFT Studies. *J. Photochem. Photobiol., A* **2014**, *277*, 37−44.
(46) Yang, Z.; Rodgers, M. T. Theoretical Studies of the Unimolecular and Bimolecular Tautomerization of Cytosine. *Phys. Chem. Chem. Phys.* **2004**, *6*, 2749−2757.
(47) Pinto, R. M.; Dias, A. A.; Costa, M. L. Electronic Structure and Thermal Decomposition of 5-Methyltetrazole Studied by UV Photoelectron Spectroscopy and Theoretical Calculations. *Chem. Phys.* **2012**, *392*, 21−28.
(48) Maçôas, E. M. S.; Khriachtchev, L.; Pettersson, M.; Fausto, R.; Räsänen, M. Rotational Isomerism of Acetic Acid Isolated in Rare-Gas Matrices: Effect of Medium and Isotopic Substitution on IR-Induced Isomerization Quantum Yield and Cis−Trans Tunneling Rate. *J. Chem. Phys.* **2004**, *121*, 1331−1338.
(49) Reva, I. D.; Jarmelo, S.; Lapinski, L.; Fausto, R. IR-Induced Photoisomerization of Glycolic Acid Isolated in Low-Temperature Inert Matrices. *J. Phys. Chem. A* **2004**, *108*, 6982−6989.
(50) Pettersson, M.; Maçôas, E. M. S.; Khriachtchev, L.; Fausto, R.; Räsänen, M. Conformational Isomerization of Formic Acid by Vibrational Excitation at Energies below the Torsional Barrier. *J. Am. Chem. Soc.* **2003**, *125*, 4058−4059.
(51) Ruelle, P.; Kesselring, U. W.; Nam-Tran, H. Ab Initio Quantum-Chemical Study of the Unimolecular Pyrolysis Mechanisms of Formic Acid. *J. Am. Chem. Soc.* **1986**, *108*, 371−375.
(52) Duan, X.; Page, M. Theoretical Investigation of Competing Mechanisms in the Thermal Unimolecular Decomposition of Acetic Acid and the Hydration Reaction of Ketene. *J. Am. Chem. Soc.* **1995**, *117*, 5114−5119.
(53) Li, J.; Brill, T. B. Spectroscopy of Hydrothermal Reactions 20: Experimental and DFT Computational Comparison of Decarboxylation of Dicarboxylic Acids Connected by Single, Double and Triple Bonds. *J. Phys. Chem. A* **2002**, *106*, 9491−9498.
(54) Li, J.; Brill, T. B. Decarboxylation Mechanism of Amino Acids by Density Functional Theory. *J. Phys. Chem. A* **2003**, *107*, 5993−5997.
(55) Takahashi, O.; Saito, K. A Theoretical Study of the Bifurcation Reaction-II: Acetic Acid. *J. Mol. Struct.: THEOCHEM* **2002**, *584*, 249−256.
(56) Moreira, I. D. P. R. Performance of Simplified G2Model Chemistry Approaches in the Study of Unimolecular Mechanisms: Thermal Decomposition of Acetic Acid in Gas Phase. *J. Mol. Struct.* **1999**, *466*, 119−126.
(57) Stoikova, M.; Oh, M.; Donaldson, D. J. Overtone-Induced Decarboxylation: A Potential Sink for Atmosheric Diacids. *J. Phys. Chem. A* **2005**, *109*, 597−602.
(58) Dunn, M. E.; Shields, G. C.; Takahashi, K.; Skodje, R. T.; Vaida, V. Experimental and Theoretical Study of the OH Vibrational Spectra and Overtone Chemistry of Gas-Phase Vinylacetic Acid. *J. Phys. Chem. A* **2008**, *112*, 10226−10235.
(59) Vaida, V.; Feierabend, K. J. N.; Takahashi; Rontu, K. Sunlight-Initiated Photochemistry: Excited Vibrational States of Atmospheric Chromophores. *Int. J. Photoenergy* **2008**, 138091.
(60) Takahashi, K.; Kramer, Z. C.; Vaida, V.; Skodje, R. T. Vibrational Overtone Induced Elimination Reactions Within Hydrogen-Bonded Molecular Clusters: the Dynamics of Water Catalyzed Reactions in $CH_2FOH{\cdot}(H_2O)_n$. *Phys. Chem. Chem. Phys.* **2007**, *9*, 3864−3871.
(61) Gómez-Zavaglia, A.; Reva, I. D.; Frija, L. M. T.; Cristiano, M. L. S.; Fausto, R. Molecular Structure, Vibrational Spectra and Photochemistry of 5-Mercapto-1-methyltetrazole. *J. Mol. Struct.* **2006**, *786*, 182−192.
(62) Gómez-Zavaglia, A.; Reva, I. D.; Frija, L. M. T.; Cristiano, M. L. S.; Fausto, R. Photochemistry of 1-Phenyl-tetrazolone Isolated in Solid Argon. *J. Photochem. Photobiol, . A* **2006**, *179*, 243−255.

NOTE ADDED IN PROOF

Recently a paper was published on the NIR-induced transformations of tetrazole acetic acid in nitrogen matrices by Araujo-Andrade, C.; Reva, I.; Fausto, R. *J. Chem. Phys.* **2014**, *140*, 064306.